ACS APPLIED MATERIALS & INTERFACES

Research Article

www.acsami.org

Intrinsic Photocatalytic Assessment of Reactively Sputtered TiO_2 Films

Damon Rafieian,[†] Rick T. Driessen,[†] Wojciech Ogieglo,[‡] and Rob G.H. Lammertink*[,†]

[†]Soft Matter, Fluidics and Interfaces, MESA+ Institute for Nanotechnology, Faculty of Science and Technology, University of Twente, P.O. Box 217, 7500AE Enschede, The Netherlands

[‡]Inorganic Membranes, MESA+ Institute for Nanotechnology, Faculty of Science and Technology, University of Twente, P.O. Box 217, 7500AE Enschede, The Netherlands

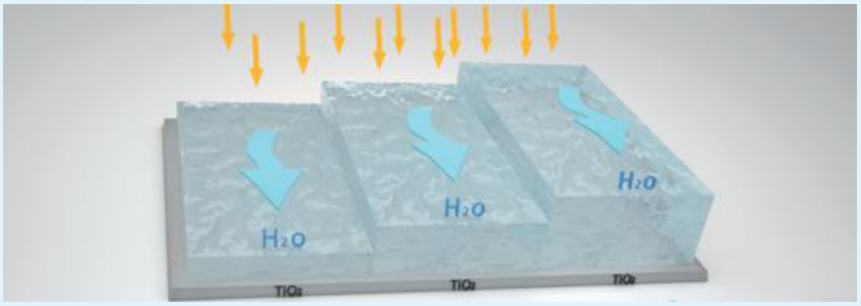

ABSTRACT: Thin TiO_2 films were prepared by DC magnetron reactive sputtering at different oxygen partial pressures. Depending on the oxygen partial pressure during sputtering, a transition from metallic Ti to TiO_2 was identified by spectroscopic ellipsometry. The crystalline nature of the film developed during a subsequent annealing step, resulting in thin anatase TiO_2 layers, displaying photocatalytic activity. The intrinsic photocatalytic activity of the catalysts was evaluated for the degradation of methylene blue (MB) using a microfluidic reactor. A numerical model was employed to extract the intrinsic reaction rate constants. High conversion rates (90% degradation within 20 s residence time) were observed within these microreactors because of the efficient mass transport and light distribution. To evaluate the intrinsic reaction kinetics, we argue that mass transport has to be accounted for. The obtained surface reaction rate constants demonstrate very high reactivity for the sputtered TiO_2 films. Only for the thinnest film, 9 nm, slightly lower kinetics were observed.

KEYWORDS: *reactive sputtering, photocatalysis, TiO_2 thin film, intrinsic reaction rate constant, microreactor*

1. INTRODUCTION

Heterogeneous photocatalysis using semiconductors finds increasing interest related to self-cleaning, water purification, and air cleaning applications.[1,2] From many semiconductors, TiO_2 is the most studied one regarding photocatalysis. Light with energy equal or higher than the band gap energy of TiO_2 leads to the formation of electron−hole pairs. The generated electron−hole pairs can in turn decompose organic contaminants via diverse reaction schemes. TiO_2 has three well-known crystal structures; anatase, rutile, and brookite. The photocatalytic performance of the anatase and rutile structures has been subjected to extensive research.[3,4] The anatase phase has a band gap of 3.2 eV, which corresponds to a wavelength of 385 nm.[1,4] The anatase phase is formed at temperatures below 400−600 °C while above 800 °C the rutile phase appears.[5] Furthermore, the formation of smaller grains at lower temperature leads to better photocatalytic activity. For grains below 10 nm, however, boundaries affect the photocatalytic activity unfavorably by increasing the recombination rate. This explains the reduced photocatalytic activity observed in amorphous TiO_2.[6]

Titanium dioxide thin films can be synthesized by techniques, such as sol−gel,[7] suspension coating,[8] electron beam evaporation,[9] electrochemical deposition,[10] different sputtering configurations,[11,12] pulsed laser deposition (PLD),[13] and many other methods.[14,15] Among them, reactive magnetron sputtering is of paramount interest since the morphology, composition, and crystallinity can be accurately controlled by modifying the deposition conditions. The resulting TiO_2 thin films present high uniformity over large areas which makes them attractive for both applications and fundamental studies as well. Hence there is a rapidly growing literature on utilizing sputtered TiO_2 thin films for photocatalytic studies.[16−18] Mostly, the main focus is directed toward the structure of the thin film as a result of different process variables and sputtering configurations.[6]

It is remarkable to observe that throughout literature, many photocatalytic degradations using sputtered TiO_2 films are characterized by just presenting the concentration versus

Received: February 3, 2015
Accepted: April 6, 2015
Published: April 6, 2015

DOI: 10.1021/acsami.5b01047
ACS Appl. Mater. Interfaces 2015, 7, 8727−8732

time[19,20] or assuming first-order bulk reaction kinetics.[21−24] The latter approach relates $\ln(c_0/c)$ to the reaction time, to obtain the apparent (volumetric) reaction rate constant which is then expressed in s^{-1}. To obtain the apparent surface reaction rate constant, one should multiply this bulk reaction rate constant k with the reactor volume to catalyst surface area ratio. Here, we will argue that besides the introduction of the volume/area ratio, mass transport has to be accounted for when evaluating the photocatalytic activity of immobilized TiO_2 thin films. The degradation of methylene blue (MB) is analyzed using dense and thin TiO_2 films within a microfluidic reactor, where we account for mass transport. By quantifying the reaction and diffusion rates in terms of the second Damköhler number, we demonstrate the fast photocatalytic kinetics and consequently the need for mass transport inclusion.

2. EXPERIMENTAL SECTION

2.1. Photocatalyst Synthesis. Silicon wafer p-type (100) as the substrate was cleaned in 98% nitric acid for 10 min and followed by rinsing and drying prior to deposition. TiO_2 thin films were prepared using a custom-made DC magnetron sputtering system (TCOATER, MESA+ Nanolab) in cleanroom environment. A 10 cm diameter titanium disk of 99.7% purity was used as the deposition target. The substrate-target distance was set at 4.4 cm and the substrate rotated at 5 rpm during the whole deposition process for enhanced uniformity. The sputtering chamber was evacuated to a base pressure of 10^{-7} mbar at room temperature prior to the deposition. A mixture of 99.5% pure oxygen and 99.99% pure argon were used as the sputtering and reactive gas, respectively. The total process pressure was regulated at 6×10^{-3} mbar in all the experiments. The target was powered by a variable DC-power supply at 500 W and presputtered for 2 min with a shutter covering the substrates in all experimental trials. No extra heating and biasing were applied to substrates in all of the depositions steps. After the sputtering, the silicon wafer was diced into 24 × 17 mm chips (Dicing saw Disco DAD 321). Some chips were annealed in an atmospheric environment for 8 h at 500 °C with heating and cooling rates of 2 °C min^{-1}.

2.2. Catalyst Layer Characterization. The morphology of the thin films was analyzed by high resolution scanning electron microscopy (Analysis Zeiss MERLIN HR-SEM). Thickness measurements were carried out by a variable angle spectroscopic ellipsometer (Woollam M2000-UI) and surface profiler (Bruker Dektak 150). The ellipsometry data was analyzed using the b-spline model to extract optical properties of the thin films.[25] The crystal structure of the thin films was investigated by XRD (Bruker D2) using CuK-α radiation at 40 kV and 40 mA working in the θ-2θ mode.

2.3. Microreactor Fabrication. A microstructured mold was made by standard photolithography using negative photoresist (SU-8) in cleanroom environment. SU-8 was spun on silicon wafer at 500 rpm for 10 s and continued to 100 rpm for 30 s. Then the sample was prebaked at 50, 65, and 95 °C for 10, 10, and 45 min, respectively. This was followed by UV exposure for 33 s and post baking at 50, 65, and 80 °C for 5, 10, and 20 min, respectively. Finally the sample was spray developed by RER 600. The SU-8 height was measured by an optical profiler (Bruker WLI Contour GT-I). Polydimethylsiloxane (PDMS) was prepared by mixing the polymer base (Permacol RTV-615 A) with the curing agent (Permacol RTV-615 B) in a 10:1 mass ratio, followed by degassing in a desiccator. The PDMS was cast on the mold and further degassed in a desiccator and cured at 60 °C for 45 min. The PDMS slab was removed from the mold and inlets and outlets were punctured. Subsequently, it was attached to the TiO_2 substrate. To ensure a leakfree assembly, additional PDMS was slightly precured and poured at the edge of the previously cured PDMS cap and further cured overnight. The fabrication steps are schematically illustrated in Figure 1. The channel has a rectangular cross section with basic dimensions of 50 μm height, 500 μm width and 5.96 cm length, giving a total volume of 1.49 μL.

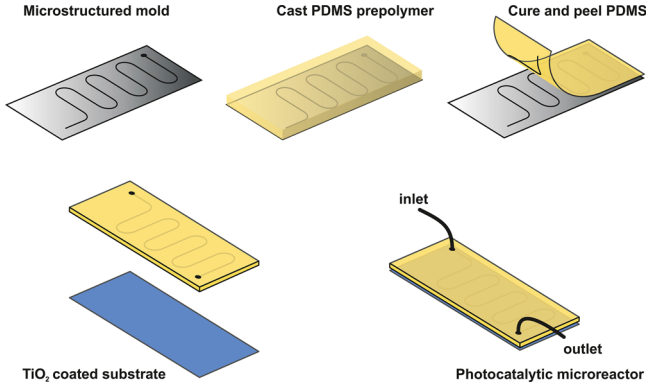

Figure 1. Illustration of the microreactor fabrication. The flow channel is defined in PDMS, which is subsequently connected to the photocatalytic surface.

2.4. Microreactor Operation. An aqueous solution of 40 μM MB (Sigma-Aldrich) was injected into the microreactor with flow rates between 3 and 50 μL min^{-1} using a syringe pump (New Era NE-4000). The MB concentration at the outlet was determined by light absorbance measurements using an in-line UV−vis spectrometer (USB2000+ Miniature Fiber Optic Ocean Optics). The monitored wavelength was 664 nm, corresponding to the maximum absorption peak of MB. The calibration was carried out for different concentrations of MB solutions and used to convert the observed absorbance to concentration. The degradation experiments were carried our using a UV light source (HP-120 Opystec Dr. Gröbel) fixed at a distance of 4 cm from the catalyst surface providing 100 mW/cm^2 photon flux density at 365 nm wavelength.

3. MODEL

To establish a fair comparison between different catalysts, the activity assessment is based on obtaining intrinsic reaction rate constants. Here we present a model that describes convection and diffusion for the flow channel combined with a surface reaction term as a boundary condition. The inclusion of the diffusion term makes sure that mass transport limitations are captured as well. The intrinsic reaction rate constant per unit surface area of the catalyst can be extracted by fitting the numerical model to the experimental data.

The 2D model of the microchannel is schematically summarized in Figure 2. The assumptions for this model are

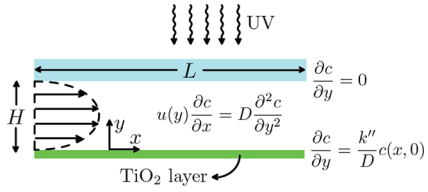

Figure 2. Representation of the 2D convection diffusion model. Convection is governed by the parabolic flow profile $u(y)$, while diffusion is only accounted for in the y direction. A first order surface reaction rate is included as the lower boundary condition.

(a) the flow is steady, laminar, and incompressible, (b) the diffusion coefficient is independent of the concentration, and (c) thermal effects are neglected.

The mass transport of the model compound in the flow channel is determined by advection (only in x direction) and diffusion (only in y direction):

DOI: 10.1021/acsami.5b01047
ACS Appl. Mater. Interfaces 2015, 7, 8727−8732

$$u(y)\frac{\partial c}{\partial x} = D\frac{\partial^2 c}{\partial y^2} \quad (1)$$

In this equation, $u(y)$ is the fluid velocity, $c(x,y)$ is the reactant concentration, and D is the molar diffusion coefficient of the model compound in water. The flow is laminar (as $10^{-4} \leq Re \leq 10^{-3}$) hence a parabolic velocity profile can be applied:

$$u(y) = u_{avg}\left(\frac{-6y^2}{H^2} + \frac{6y}{H}\right) \quad (2)$$

The parabolic velocity profile is obtained by solving the Navier–Stokes equation for two parallel flat plates in 2D with laminar flow for the coordinate system shown in Figure 2. As our physical device contains channels with a width to height ratio of 10, this is a fair approximation.

At $x = 0$ the concentration is equal to the inlet concentration c_0 for all y:

$$c|_{x=0} = c_0 \quad (3)$$

The upper wall ($y = H$) is considered impermeable, represented by the Neumann boundary condition:

$$\frac{\partial c}{\partial y}|_{y=H} = 0 \quad (4)$$

For the boundary condition at the lower wall ($y = 0$), the molar flux to the catalyst surface is equal to the rate of consumption of the model compound. Assuming a first-order reaction, the boundary condition reads

$$D\frac{\partial c}{\partial y}|_{y=0} = k''c|_{y=0} \quad (5)$$

where k'' is the intrinsic surface reaction rate constant (m s^{-1}). k'' relates to the "bulk" k (s^{-1}) constant by taking the reactor volume to catalyst surface into account: $k'' = k(V/A)$.

The equations for the flow channel (1 and 2) and the boundary conditions (4 and 5) are nondimensionalized to yield

$$u_{avg}(-6\tilde{y}^2 + 6\tilde{y})\frac{H^2}{LD}\frac{\partial \tilde{c}}{\partial \tilde{x}} = \frac{\partial^2 \tilde{c}}{\partial \tilde{y}^2} \quad (6)$$

$$\tilde{c}|_{\tilde{x}=0} = 1 \quad (7)$$

$$\frac{\partial \tilde{c}}{\partial \tilde{y}}|_{\tilde{y}=1} = 0 \quad (8)$$

$$\frac{\partial \tilde{c}}{\partial \tilde{y}}|_{\tilde{y}=0} = \frac{k''H}{D}\tilde{c} = Da_{II}\tilde{c} \quad (9)$$

where $\tilde{c} = c/c_0$, $\tilde{x} = x/L$, and $\tilde{y} = y/H$. Da_{II} is the second Damköhler number defined as the ratio between the chemical reaction rate and the diffusive mass transport.[26] The model is solved numerically in MATLAB using the pdepe solver. The mesh was refined until mesh-independent solutions were obtained. The mixing cup concentration of the outflow was matched to the experimental value, while only k'' was varied.

4. RESULTS AND DISCUSSION

4.1. Film Deposition and Characterization. Figure 3a shows the sputtering rate as a function of oxygen partial pressure at constant total pressure (6×10^{-3} mbar). There is a sharp drop in the sputtering rate at an oxygen partial pressure of 8.57×10^{-4} mbar. This transition in sputtering rate typically

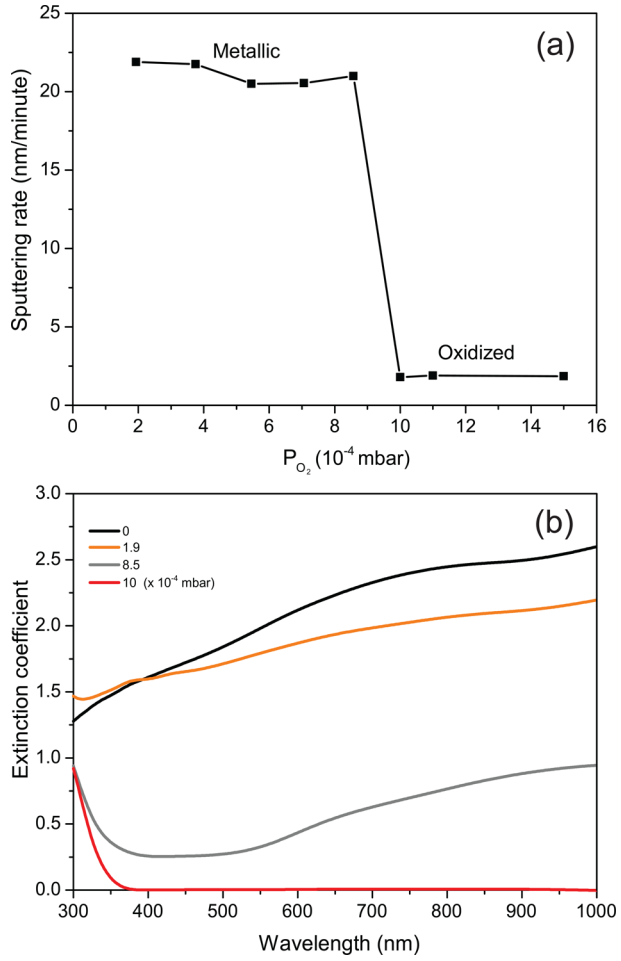

Figure 3. (a) Sputtering deposition rate and (b) extinction coefficient of thin films sputtered at different oxygen partial pressures.

indicates that the deposited material transits from a metallic to an oxidized form. We extract the extinction coefficient of the deposited thin films at different oxygen partial pressures. As observed in Figure 3b, the extinction coefficient of the deposited films is the highest for the pure titanium and it gradually decreases until complete transparency in the visible region for the film prepared at 10^{-3} mbar. It is exactly at this oxygen partial pressure that the stoichiometric TiO_2 is formed with absorption in the UV region of the light spectrum.[27] No further differences in terms of extinction coefficient were observed at higher oxygen partial pressures.

Figure 4 depicts the effect of annealing on the surface morphology of the TiO_2 thin film deposited at 10^{-3} mbar. The insets display the corresponding X-ray diffraction patterns. The as-deposited film at room temperature is amorphous due to the lack of energy for mobilization of the nucleated particles and formation of crystals with a regular lattice.[27] After annealing, grains are formed and the diffraction peak for 101 (anatase) appears. Despite the crystallization during annealing, no significant differences were observed in terms of extinction coefficient. The refractive index of the thin film only increased slightly upon annealing. According to Horprathum et al. this is caused by the reaction between amorphous TiO_2 with previously diffused oxygen and densification of the film.[28]

4.2. Photocatalytic Performance. Despite the comparable extinction coefficients for TiO_2 thin films before and after annealing, the photocatalytic activity differs tremendously.

DOI: 10.1021/acsami.5b01047
ACS Appl. Mater. Interfaces 2015, 7, 8727–8732

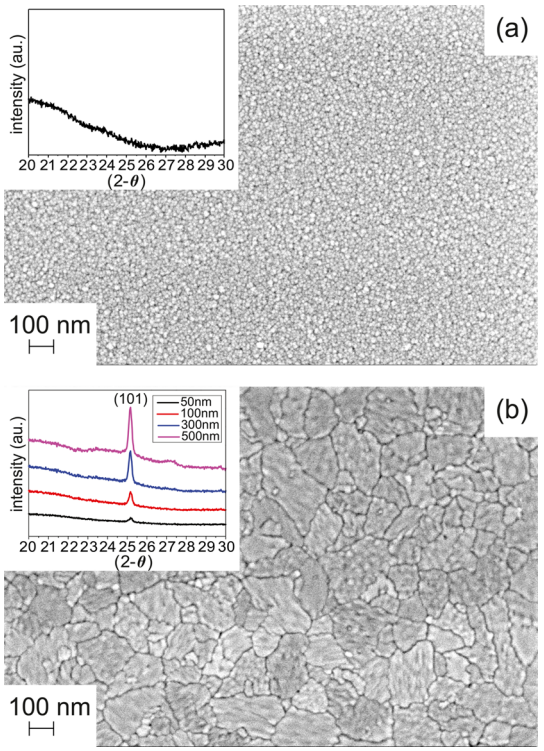

Figure 4. Microstructure and XRD patterns of TiO_2 thin film before (a) and after annealing at 500 °C for 8 h (b). The assigned peak to the (101) plane is present in all of the film thicknesses.

Amorphous thin films display no photocatalytic activity. Possibly, lattice defects generate trap sites for the photogenerated electron−holes, which increase the recombination rate.[6] Figure 5 shows the degradation of MB (40 μM) in the microreactor as a function of residence times utilizing the catalyst sputtered at 10^{-3} mbar oxygen partial pressure followed by annealing (Figure 4b). The concentration of MB was determined by UV−vis absorbance for different residence times (Figure 5 insert). The degradation is calculated by the following equation:

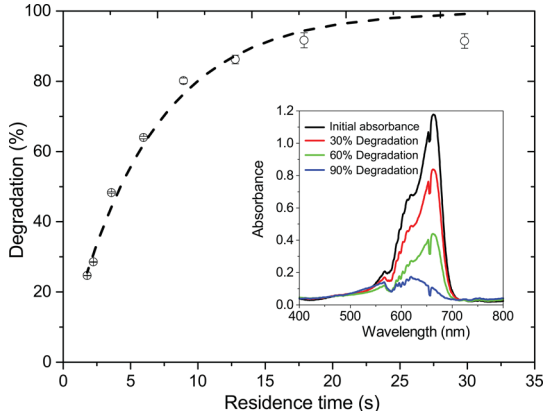

Figure 5. Degradation of methylene blue (40 μM) as a function of residence time. The fit results from the numerical model using a single fitted surface reaction rate constant (k'' = 1.1× 10^{-5} m s^{-1}). The inset shows the initial absorbance spectra (black) and at 30% (red), 60% (green), and 90% (blue) degradation for methylene blue.

$$\text{degradation} = \frac{c_0 - c_f}{c_0} \times 100\% \tag{10}$$

where c_0 and c_f are the inlet and outlet concentrations, respectively. The fitted line corresponds to the results of the numerical model. Note that only the surface reaction rate constant k'' is adjusted to fit the experimental data, and that mass transport is accounted for by the convection diffusion equation. The standard deviation in degradation is based on the standard deviation of the initial and final concentration. At larger residence times, this standard deviation increases because of the low measured concentration and the long time required to reach steady state. The fitted reaction rate constant k is 0.22 s^{-1} (k'' = 1.1× 10^{-5} m s^{-1}) based on the molecular diffusion of MB in water (D = 5.7× 10^{-10} m^2 s^{-1}).[8]

Table 1 represents the photocatalytic reaction rate constants of reactively sputtered TiO_2 films reported in literature and our findings. Throughout literature, photocatalytic performance is most frequently quantified by the apparent reaction rate constant, that is, by determining the slope of ln (c_0/c_f) versus t. This reaction rate constant represents the volume based conversion and does not take the catalyst area per reactor volume into account. It is therefore not suitable to compare catalysts when these have been assessed with different reactor configurations. A better comparison involves the presentation of a surface normalized reaction rate, obtained by multiplying the "bulk" rate constant k with the reactor volume to catalyst area ratio. In our presented case, this concerns the height of the microchannel H.

The extracted surface reaction rate constant for our sputtered film is at least an order of magnitude larger compared to previously reported values. Besides the possible deviations in active surface area and illumination intensities, mass transport limitations can be responsible for the observed difference. Below, we will address the significance of mass transport further, by discussing the second Damköhler number. The extracted rate constant per unit surface area (k'' = 1.1× 10^{-5} m s^{-1}) is also 100 times higher than the value reported for MB degradation using a porous film, obtained by a spin-coated commercial TiO_2 suspension (k'' = 2.07× 10^{-7} m s^{-1}).[8] A porous film evidently suffers from incomplete usage of the photocatalyst surface because of either light penetration or mass diffusion limitation.[8]

To determine the regime where the rate of reaction is dependent on the chemical reaction or the mass transfer, the microreactor is modeled for various values of second Damköhler number, which is defined as the ratio between the chemical reaction rate and the diffusive mass transport rate (eq 11).[26]

$$Da_{II} = \frac{\text{reaction rate}}{\text{diffusive mass transfer rate}} = \frac{k''H}{D} \tag{11}$$

Apparently, when $Da_{II} \gg 1$ the chemical reaction rate is faster than transport of reactants to the catalyst and as a result the reaction rate becomes mass transport limited. Already for our microreactor, which displays efficient mass transport because of the small channel size, we obtain a Da_{II} close to unity.

On the basis of the reported values in the literature, as presented in Table 1, typical Damköhler numbers much larger than unity can be realized. For such cases, the diffusive mass transport would be severely limiting. The mass transfer rate can be enhanced by convection (e.g., by stirring or flow) in order to reduce the diffusive boundary layer. Often the actual flow or

DOI: 10.1021/acsami.5b01047
ACS Appl. Mater. Interfaces 2015, 7, 8727−8732

Table 1. Overall (k) and Surface Normalized (k'') Photocatalytic Reaction Rate Constant of Sputtered TiO_2

sputtering deposition	k (s^{-1})	k'' (m s^{-1})	volume/area (m)	ref
RF magnetron	3.09×10^{-5}	4.96×10^{-7}	1.60×10^{-2}	24
RF magnetron	1.92×10^{-4}	2.87×10^{-6}	1.5×10^{-2}	20
pulsed DC	2.83×10^{-5}	1.89×10^{-6}	6.67×10^{-2}	23
unbalanced DC	1.99×10^{-5}	7.99×10^{-8}	2.5×10^{-3}	19
RF magnetron	1.58×10^{-7}	4.22×10^{-8}	2.67×10^{-1}	22
DC magnetron	2.2×10^{-1}	1.1×10^{-5}	5.0×10^{-5}	this work

stirring conditions are not mentioned in literature, which makes the identification of potential mass transfer limitations impossible.

Figure 6 shows the degradation of MB as a function of second Damköhler number ranging from 10^{-3} to 10^{4} and the

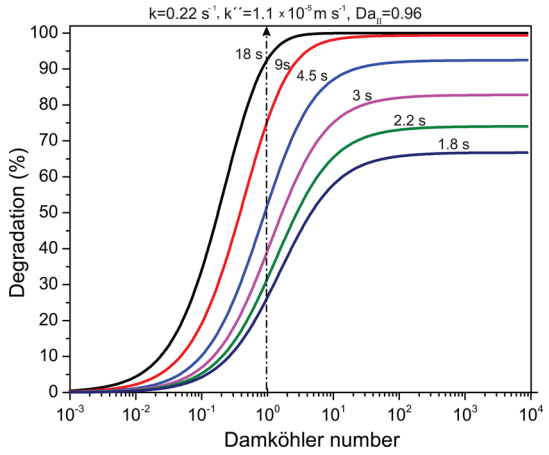

Figure 6. Degradation of MB as a function of second Damköhler number for the multiple residence times as computed by the model for the microreactor. The dashed line indicates the calculated second Damköhler based on the extracted reaction rate constant.

dashed line indicates the calculated second Damköhler number based on our obtained $k'' = 1.1 \times 10^{-5}$ m s^{-1}, microchannel height (H) and the diffusion coefficient (D) for MB. The microreactor operates in the transition of mass transfer limited and reaction limited region as the value for second Damköhler number is 0.96. This number can be used to assess the severance of mass transport limitations. Most easily, one can extract a height H for $Da_{II} \simeq 1$ that indicates a critical diffusive boundary layer thickness.

The effect of TiO_2 film thickness on the photocatalytic performance was investigated. We prepared TiO_2 thin films from 9 to 500 nm thickness and measured the degradation of MB at a single residence time of 1.78 s (50 μL min^{-1}). As observed in Figure 7, catalysts thicker than 50 nm exhibit constant photocatalytic activity. In literature, different minimal thicknesses are reported ranging from 140 to 300−350 nm.[6,29] In order to study the effect of film thickness intrinsically, it is of paramount importance that the surface morphology of the film does not change with film thickness. Luttrel et al. prepared thin anatase films utilizing high-quality epitaxial TiO_2 films and evaluated the photocatalytic activity. They showed that the photocatalytic activity remained constant down to ∼5 nm due to the diffusion length of the charge carriers.[4] According to the HRSEM (Figure 7) the surface morphology of the thin films changes at 50 nm thickness. The density of the grains and as a result grain boundaries are significantly lower for the 9 nm thin

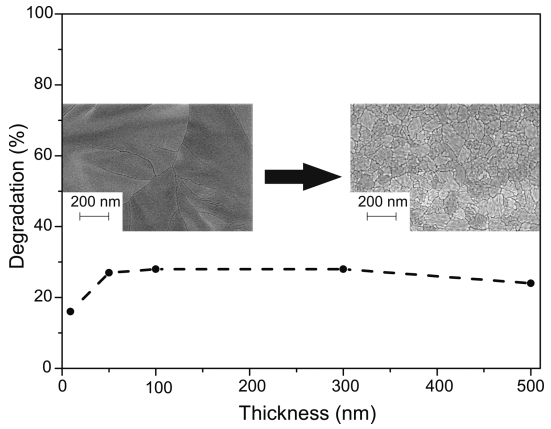

Figure 7. Photocatalytic degradation (at 1.78 s residence time) of MB as a function of catalyst thickness. The inserted HRSEM displays the surface morphology of a 9 nm (left) and a 50 nm (right) thin film.

film compared to the films thicker than 50 nm. The extracted reaction rate constant for the 9 nm thin catalyst is $k'' = 7.3 \times 10^{-6}$ m s^{-1} which is only about a third lower compared to the thicker layers.

5. CONCLUSION

TiO_2 was deposited by DC reactive magnetron sputtering at different oxygen partial pressures. A clear transition was observed as a function of the oxygen partial pressure between deposition of a metallic and an oxide film. The optical properties of the thin films were investigated by ellipsometry. After thermal annealing, anatase was formed, as identified by XRD. The performance of the photocatalyst was investigated in a microfluidic reactor by degradation of methylene blue for different residence times. ∼90% degradation was achieved within 20 s and a surface reaction rate constant of 1.1×10^{-5} m s^{-1} was extracted. This is at least 1 order of magnitude higher than what reported in other studies. The photocatalytic activity of the sputtered TiO_2 films is independent of thicknesses down to 50 nm at least. We present a numerical model that is capable to extract the intrinsic reaction rate constant. Furthermore, the model provides insight regarding possible mass transport limitations, verified by the second Damköhler number. This approach allows an intrinsic comparison of photocatalytic kinetic data.

AUTHOR INFORMATION

Corresponding Author

*Phone: +31 (0)534894798. Fax: +31 (0)534892882. E-mail: r.g.h.lammertink@utwente.nl.

Notes

The authors declare no competing financial interest.

DOI: 10.1021/acsami.5b01047
ACS Appl. Mater. Interfaces 2015, 7, 8727−8732

■ ACKNOWLEDGMENTS

This work is supported by NanoNextNL, a micro and nanotechnology consortium of the Government of The Netherlands and 130 partners.

■ REFERENCES

(1) Linsebigler, A. L.; Lu, G.; Yates, J. T. Photocatalysis on TiO_n Surfaces: Principles, Mechanisms, and Selected Results. *Chem. Rev.* **1995**, *95*, 735−758.
(2) Fujishima, A.; Honda, K. Electrochemical Photolysis of Water at a Semiconductor Electrode. *Nature* **1972**, *238*, 37−38.
(3) Banerjee, S.; Gopal, J. Physics and Chemistry of Photocatalytic Titanium dioxide: Visualization of Bactericidal Activity using Atomic Force Microscopy. *Curr. Sci.* **2006**, *90*, 1378−1383.
(4) Luttrell, T.; Halpegamage, S.; Tao, J.; Kramer, A.; Sutter, E.; Batzill, M. Why is Anatase a Better Photocatalyst than Rutile? Model Studies on Epitaxial TiO_2 Films. *Sci. Rep.* **2014**, *4*, 4043.
(5) Hanaor, D. A. H.; Sorrell, C. C. Review of the Anatase to Rutile Phase Transformation. *J. Mater. Sci.* **2010**, *46*, 855−874.
(6) Eufinger, K.; Poelman, D.; Poelman, H.; Gryse, R. D.; Marin, G. B. Effect of Microstructure and Crystallinity on the Photocatalytic Activity of TiO_2 Thin films Deposited by dc Magnetron Sputtering. *J. Phys. D: Appl. Phys.* **2007**, *40*, 5232−5238.
(7) Piveteau, L.-D.; Gasser, B.; Schlapbach, L. Evaluating Mechanical Adhesion of Sol−Gel Titanium Dioxide Coatings containing Calcium Phosphate for Metal Implant Application. *Biomaterials* **2000**, *21*, 2193−2201.
(8) Visan, A.; Rafieian, D.; Ogieglo, W.; Lammertink, R. G. H. Modeling Intrinsic Kinetics in Immobilized Photocatalytic Microreactors. *Appl. Catal., B* **2014**, *150−151*, 93−100.
(9) Yang, T.-S.; Shiu, C.-B.; Wong, M.-S. Structure and Hydrophilicity of Titanium Oxide Films prepared by Electron Beam Evaporation. *Surf. Sci.* **2004**, *548*, 75−82.
(10) Manivannan, A.; Spataru, N.; Arihara, K.; Fujishima, A. Electrochemical Deposition of Titanium Oxide on Boron-Doped Diamond Electrodes. *Electrochem. Solid-State Lett.* **2005**, *8*, C138.
(11) Williams, L. M. Structural Properties of Titanium Dioxide Films Deposited in an rf Glow Discharge. *J. Vac. Sci. Technol., A* **1983**, *1*, 1810.
(12) Kubart, T.; Jensen, J.; Nyberg, T.; Liljeholm, L.; Depla, D.; Berg, S. Influence of the Target Composition on Reactively Sputtered Titanium Oxide Films. *Vacuum* **2009**, *83*, 1295−1298.
(13) Suda, Y.; Kawasaki, H.; Ueda, T.; Ohshima, T. Preparation of High Quality Nitrogen Doped TiO_2 Thin Film as a Photocatalyst using a Pulsed Laser Deposition Method. *Thin Solid Films* **2004**, *453−454*, 162−166.
(14) O'Neill, S. A.; Parkin, I. P.; Clark, R. J. H.; Mills, A.; Elliott, N. Atmospheric Pressure Chemical Vapour Deposition of Titanium Dioxide Coatings on Glass. *J. Mater. Chem.* **2003**, *13*, 56−60.
(15) Aarik, J.; Aidla, A.; Mändar, H.; Uustare, T. Atomic Layer Deposition of Titanium Dioxide from $TiCl_4$ and H_2O: Investigation of Growth Mechanism. *Appl. Surf. Sci.* **2001**, *172*, 148−158.
(16) Yamagishi, M.; Kuriki, S.; Song, P.; Shigesato, Y. Thin film TiO_2 Photocatalyst Deposited by Reactive Magnetron Sputtering. *Thin Solid Films* **2003**, *442*, 227−231.
(17) Dumitriu, D.; Bally, A. R.; Ballif, C.; Hones, P.; Schmid, P.; Sanjinés, R.; Lévy, F.; Pârvulescu, V. Photocatalytic Degradation of Phenol by TiO_2 Thin Films Prepared by Sputtering. *Appl. Catal., B* **2000**, *25*, 83−92.
(18) Takeda, S.; Suzuki, S.; Odaka, H.; Hosono, H. Photocatalytic TiO_2 Thin film Deposited onto Glass by DC Magnetron Sputtering. *Thin Solid Films* **2001**, *392*, 338−344.
(19) Chiu, S.-M.; Chen, Z.-S.; Yang, K.-Y.; Hsu, Y.-L.; Gan, D. Photocatalytic Activity of Doped TiO_2 Coatings prepared by Sputtering Deposition. *J. Mater. Process. Technol.* **2007**, *192−193*, 60−67.
(20) Pihosh, Y.; Goto, M.; Kasahara, A.; Tosa, M. Photocatalytic Property of TiO_2 Thin films Sputtered-Deposited on Unheated Substrates. *Appl. Surf. Sci.* **2009**, *256*, 937−942.
(21) Yu, J.; Zhao, X. Effect of Surface Treatment on the Photocatalytic Activity and Hydrophilic Property of the Sol−Gel Derived TiO_2 Thin Films. *Mater. Res. Bull.* **2001**, *36*, 97−107.
(22) Sangpour, P. Photoenhanced Degradation of Methylene blue on Cosputtered M: TiO_2 (M = Au, Ag, Cu) Nanocomposite Systems: A Comparative Study. *J. Phys. Chem. C* **2010**, *2*, 13955−13961.
(23) Ratova, M.; Kelly, P.; West, G.; Iordanova, I. Enhanced Properties of Magnetron Sputtered Photocatalytic Coatings via Transition Metal Doping. *Surf. Coat. Technol.* **2013**, *228*, S544−S549.
(24) Nair, P. B.; Daniel, G. P.; Joy, K.; Ramakrishnan, V.; Kumar, D. D.; Thomas, P. Structural, Optical, Photoluminescence and Photocatalytic Investigations on Fe-Doped TiO_2 Thin films. *Thin Solid Films* **2014**, *550*, 121−127.
(25) Johs, B.; Hale, J. S. Dielectric Function Representation by B-Splines. *Phys. Status Solidi A* **2008**, *205*, 715−719.
(26) Bird, R. B.; Stewart, W. E.; Lightfoot, E. N. *Transport Phenomena*, 2nd ed.; John Wiley & Sons, Inc.: Hoboken, NJ, 2007; pp 543−581.
(27) Tavares, C.; Vieira, J.; Rebouta, L.; Hungerford, G.; Coutinho, P.; Teixeira, V.; Carneiro, J.; Fernandes, A. Reactive Sputtering Deposition of Photocatalytic TiO_2 Thin films on Glass Substrates. *Mater. Sci. Eng., B* **2007**, *138*, 139−143.
(28) Horprathum, M. A Spectroscopic Ellipsometry Study of TiO_2 Thin films Prepared by dc Reactive Magnetron Sputtering: Annealing Temperature Effect. *Chin. Phys. Lett.* **2007**, *24*, 1505.
(29) Tada, H.; Tanaka, M. Dependence of TiO_2 Photocatalytic Activity upon its Film Thickness. *Langmuir* **1997**, *13*, 360−364.

DOI: 10.1021/acsami.5b01047
ACS Appl. Mater. Interfaces 2015, 7, 8727−8732